*Appl. Math. Mech. -Engl. Ed.*, **32**(12), 1587–1598 (2011)
DOI 10.1007/s10483-011-1525-6


**Applied Mathematics and Mechanics (English Edition)**

# Stokes flow of micro-polar fluids by peristaltic pumping through tube with slip boundary condition*

D. TRIPATHI[1], M. K. CHAUBE[2], P. K. GUPTA[3]

(1. Department of Mathematics, Indian Institute of Technology Ropar, Punjab 140001, India;
2. Department of Mathematics, Raj Kumar Goel Institute of Technology, Ghaziabad 201001, India;
3. Department of Applied Mathematics, Institute of Technology, Banaras Hindu University, Varanasi 221005, India)

**Abstract** This paper studies the Stokes flow of micro-polar fluids by peristaltic pumping through the cylindrical tube under the effect of the slip boundary condition. The motion of the wall is governed by the sinusoidal wave equation. The analytical and numerical solutions for the axial velocity, the micro-polar vector, the stream function, the pressure gradient, the friction force, and the mechanical efficiency are obtained by using the lubrication theory under the low Reynolds number and long wavelength approximations. The impacts of the emerging parameters, such as the coupling number, the micro-polar parameter, the slip parameter on pumping characteristics, the friction force, the velocity profile, the mechanical efficiency, and the trapping phenomenon are depicted graphically. The numerical results infer that large pressure is required for peristaltic pumping when the coupling number is large, while opposite behaviors are found for the micro-polar parameter and the slip parameter. The size of the trapped bolus reduces with the increase in the coupling number and the micro-polar parameter, whereas it blows up with the increase in the slip parameter.

**Key words** Stokes flow, slip boundary condition, mechanical efficiency, micro-polar fluid, peristaltic pumping, trapping

**Chinese Library Classification** O357.4
**2010 Mathematics Subject Classification** 76D08

## 1 Introduction

It is well known that most physiological fluids are non-Newtonian. Micro-polar fluids are a special type of non-Newtonian fluids, which was first introduced by Eringen[1]. They represent the fluids consisting of rigid randomly oriented (or spherical) particles suspended in a viscous medium, where the deformation of the particles is ignored. Micro-polar fluids exhibit some microscopic effects arising from the local structure and micro-motion of the fluid elements. They can sustain couple stresses.

Peristaltic pumping is a common phenomenon. It is the pumping of the fluid induced due to the progressive waves of contraction or expansion and traveling along the walls of the vessel

* Received Jan. 30, 2011 / Revised Jul. 18, 2011
Corresponding author D. TRIPATHI, Professor, Ph. D., E-mail: dtripathi.rs.apm@itbhu.ac.in

containing the fluid. It occurs in the urine flow from kidney to bladder, the intra-uterine fluid motion, the swallowing food through the esophagus and so on.

The peristaltic motion of micro-polar fluids through a cylindrical tube was first studied by Devi and Devanathan[2]. This study was further improved with different wall properties and different flow regions[3–11]. The peristaltic transport of incompressible fluids (Newtonian and few non-Newtonian) has been reported in Refs. [12–16].

The flow of fluids with small inertial forces, compared with viscous forces, is known as Stokes flow, which is also called creeping flow. In Stokes flow, the Reynolds number, the length scale, and the fluid velocities are very low, while the viscosity is very large. The swimming of microorganisms and sperm, the movement of food bolus through alimentary canal, and the flow of lava in nature are applicable examples of Stokes flow. Stokes flow of non-Newtonian fluids through different geometries of the flow pattern by peristaltic pumping have recently been reported in Refs. [17–29].

However, all the problems studied in the above literatures are formulated without the slip boundary condition. In fact, there is always a certain amount of slips in real systems, which is hard to be detected experimentally because of the required space resolution. The no-slip boundary condition is a convenient idealization for the viscous fluids near walls. In view of the wide applications of the Stokes flow, the micropolar fluids, the peristaltic pumping, and the slip boundary condition in bio-fluid mechanics and industrial-fluid mechanics, we present a mathematical model incorporating all these physical and mechanical properties, and study the physical and mechanical relevance by numerical calculations. The paper is organized as follows. Section 2 presents the mathematical analysis. Section 3 gives the numerical results and discussion. The last section focuses on the main conclusion remarks.

## 2 Mathematical formulation and its solution

Let $(r', \theta', x')$ and $(r, \theta, x)$ be the reference fixed frame and the reference wave frame, respectively. Then, the transformations from the fixed frame to the wave frame are given by

$$r = r', \quad x = x' - ct, \quad v = v', \quad u = u' - c, \tag{1}$$

where $(v',\ u')$ and $(v,\ u)$ are the radial and axial velocity components in the reference fixed frame and the reference wave frame, respectively, and $c$ is the wave velocity.

The governing equations of the flow of an incompressible micro-polar fluid in the absence of body force and body couple in the reference wave frame[3–5]

$$\nabla \cdot V = 0, \tag{2}$$

$$\rho(V \cdot \nabla V) = -\nabla p + \kappa \nabla \times W + (\mu + \kappa)\nabla^2 V, \tag{3}$$

$$\rho j(V \cdot \nabla W) = -2\kappa W + \kappa \nabla \times V - \gamma(\nabla \times \nabla \times W) + (\alpha + \beta + \gamma)\nabla(\nabla \cdot W), \tag{4}$$

where $V = (v, 0, u)$ and $W = (0, \omega, 0)$ are the velocity vector and the micro-rotation vector, respectively, $p$ is the fluid pressure, $\rho$ is the fluid density, and $j$ is the micro-gyration parameter. The constants $\mu$, $\kappa$, $\alpha$, $\beta$, and $\gamma$ are material constants satisfying

$$2\mu + \kappa \geqslant 0, \quad 3\alpha + \beta + \gamma \geqslant 0, \quad \gamma \geqslant |\beta|\,. \tag{5}$$

The equation of wall motion in the reference wave frame is

$$H = a + b \sin \frac{2\pi x}{\lambda}. \tag{6}$$

We non-dimensionalize the different variables as follows:

$$\begin{cases} \overline{r} = \dfrac{r}{a}, \quad \overline{x} = \dfrac{x}{\lambda}, \quad \overline{u} = \dfrac{u}{c}, \quad \overline{v} = \dfrac{\lambda}{ca} v, \\ \overline{\omega} = \dfrac{a}{c}\omega, \quad \overline{p} = \dfrac{a^2}{\lambda c \mu} p, \quad \overline{t} = \dfrac{c}{\lambda} t, \quad h = \dfrac{H}{a}, \quad \overline{j} = \dfrac{j}{a^2}. \end{cases} \tag{7}$$

Using Eq. (7) into Eqs. (2)–(4) and (6) and dropping the bar, we get

$$\frac{\partial v}{\partial r} + \frac{v}{r} + \frac{\partial u}{\partial x} = 0, \tag{8}$$

$$Re\delta^3\Big(v\frac{\partial v}{\partial r} + u\frac{\partial v}{\partial x}\Big) = -\frac{\partial p}{\partial r} + \frac{\delta^2}{1-N}\Big(-N\frac{\partial \omega}{\partial x} + \frac{\partial^2 v}{\partial r^2} + \frac{1}{r}\frac{\partial v}{\partial r} - \frac{v}{r^2} + \delta^2\frac{\partial^2 v}{\partial x^2}\Big), \tag{9}$$

$$Re\delta\Big(v\frac{\partial u}{\partial r} + u\frac{\partial u}{\partial x}\Big) = -\frac{\partial p}{\partial x} + \frac{1}{1-N}\Big(\frac{N}{r}\frac{\partial (r\omega)}{\partial r} + \frac{\partial^2 u}{\partial r^2} + \frac{1}{r}\frac{\partial u}{\partial r} + \delta^2\frac{\partial^2 u}{\partial x^2}\Big), \tag{10}$$

$$\begin{aligned} &\frac{jRe\delta(1-N)}{N}\Big(v\frac{\partial \omega}{\partial r} + u\frac{\partial \omega}{\partial x}\Big) \\ &= -2\omega + \Big(\delta^2\frac{\partial v}{\partial x} - \frac{\partial u}{\partial r}\Big) + \frac{2-N}{m^2}\Big(\frac{\partial}{\partial r}\Big(\frac{1}{r}\frac{\partial (r\omega)}{\partial r}\Big) + \delta^2\frac{\partial^2 \omega}{\partial x^2}\Big), \end{aligned} \tag{11}$$

$$h(x) = 1 + \phi\sin(2\pi x), \tag{12}$$

where $\delta = a/\lambda$ is the wave number, $\phi = b/a$ is the amplitude, $Re = \rho ac/\mu$ is the Reynolds number, $m = \sqrt{a^2\kappa(2\mu+\kappa)/\gamma(\mu+\kappa)}$ is the micro-polar parameter, and $N = \kappa/(\mu+\kappa)$ is the coupling number ($0 \leqslant N < 1$). $\alpha$ and $\beta$ do not appear in the governing equations as the micro-rotation vector $W$ is solenoidal. In the limit $\kappa \to 0$, i.e., $N \to 0$, the governing equations reduce to the classical Navier-Stokes equations.

Applying the long wavelength assumption ($\delta \ll 1$) and the low Reynolds number approximation ($Re \to 0$) (i.e., Stokes flow), Eqs. (8–11) reduce to

$$\frac{\partial v}{\partial r} + \frac{v}{r} + \frac{\partial u}{\partial x} = 0, \tag{13}$$

$$\frac{\partial p}{\partial r} = 0, \tag{14}$$

$$\frac{N}{r}\frac{\partial (r\omega)}{\partial r} + \frac{\partial^2 u}{\partial r^2} + \frac{1}{r}\frac{\partial u}{\partial r} = (1-N)\frac{\partial p}{\partial x}, \tag{15}$$

$$2\omega + \frac{\partial u}{\partial r} - \frac{2-N}{m^2}\frac{\partial}{\partial r}\Big(\frac{1}{r}\frac{\partial (r\omega)}{\partial r}\Big) = 0. \tag{16}$$

The corresponding boundary conditions in the wave frame are as follows:

(i) The regularity condition is

$$\frac{\partial u}{\partial r} = 0 \quad \text{at} \quad r = 0. \tag{17}$$

(ii) The slip boundary condition is

$$u = -1 - k_n\frac{\partial u}{\partial r} \quad \text{at} \quad r = h, \tag{18}$$

$$\omega = 0 \quad \text{at} \quad r = h, \tag{19}$$

$$u = 0, \quad \omega = 0 \quad \text{at} \quad r = 0, \tag{20}$$

where $k_n$ $(= L/a)$ is the dimensionless slip parameter, and $L$ is the dimensional slip parameter.

From Eq. (14), it is clear that $p$ is a function of $x$ only. Then, Eq. (15) may be rewritten as

$$\frac{\partial}{\partial r}\Big(r\frac{\partial u}{\partial r} + Nr\omega - (1-N)\frac{r^2}{2}\frac{\mathrm{d}p}{\mathrm{d}x}\Big) = 0. \tag{21}$$

Integrating Eq. (21) and dividing it by $r$, we get

$$\frac{\partial u}{\partial r} = (1-N)\Big(\frac{r}{2}\frac{\mathrm{d}p}{\mathrm{d}x} + \frac{C_1}{r}\Big) - N\omega. \tag{22}$$

Using Eq. (22) in Eq. (16), we get

$$\frac{\partial^2\omega}{\partial r^2} + \frac{1}{r}\frac{\partial\omega}{\partial r} - \Big(m^2 + \frac{1}{r^2}\Big)\omega = \frac{m^2(1-N)}{2-N}\Big(\frac{r}{2}\frac{\mathrm{d}p}{\mathrm{d}x} + \frac{C_1}{r}\Big). \tag{23}$$

The general solution to Eq. (23) is

$$\omega = C_2(x)\mathrm{I}_1(mr) + C_3(x)\mathrm{K}_1(mr) - \frac{1-N}{2-N}\Big(\frac{r}{2}\frac{\mathrm{d}p}{\mathrm{d}x} + \frac{C_1}{r}\Big), \tag{24}$$

where $\mathrm{I}_1(mr)$ and $\mathrm{K}_1(mr)$ are modified Bessel functions of the first and second kinds of the first-order, respectively. Substitute Eq. (24) into Eq. (22) and integrate it. Then, the axial velocity can be obtained as follows:

$$u = \frac{N}{m}(-C_2(x)\mathrm{I}_0(mr) + C_3(x)\mathrm{K}_0(mr)) + \frac{1-N}{2-N}\Big(\frac{r^2}{2}\frac{\mathrm{d}p}{\mathrm{d}x} + 2C_1(x)\log r\Big) + C_4(x), \tag{25}$$

where $\mathrm{I}_0$ and $\mathrm{K}_0$ are modified Bessel functions of the zeroth-order. Since we require $\omega$ to be finite on $r = 0$, $C_1(x) = C_2(x) = 0$ in Eq. (24). By using Eqs. (18) and (19) in Eq. (25), the solutions for the axial velocity and the micro-polar vector can be given by

$$u = -1 + \frac{1-N}{2(2-N)}\frac{\mathrm{d}p}{\mathrm{d}x}\Big(r^2 - h^2 - 2hk_n + hNk_n + \frac{Nh}{m\mathrm{I}_1(mh)}(\mathrm{I}_0(mh) - \mathrm{I}_0(mr))\Big), \tag{26}$$

$$\omega = \frac{1-N}{2(2-N)}\frac{\mathrm{d}p}{\mathrm{d}x}\Big(\frac{h\,\mathrm{I}_1(mr)}{\mathrm{I}_1(mh)} - r\Big). \tag{27}$$

The stream function $(\psi)$ is defined by

$$v = -\frac{1}{r}\frac{\partial\psi}{\partial x}, \quad u = \frac{1}{r}\frac{\partial\psi}{\partial r}. \tag{28}$$

Using Eqs. (26) and (28), we get

$$\begin{aligned}\psi = &-\frac{r^2}{2} + \frac{1-N}{2(2-N)}\frac{\mathrm{d}p}{\mathrm{d}x}\Big(\frac{r^4}{4} - \frac{h^2r^2}{2} - hk_nr^2 + \frac{hNk_n\,r^2}{2}\\ &+ \frac{Nh}{m\mathrm{I}_1(mh)}\Big(\frac{r^2}{2}\mathrm{I}_0(mh) - \frac{r}{m}\mathrm{I}_1(mr)\Big)\Big).\end{aligned} \tag{29}$$

The dimensionless flux ($q = q'a^2c/\pi$, where $q'$ is the flux in the wave frame) is given by

$$q = \int_0^h 2ru\mathrm{d}r = -h^2 - \frac{1-N}{4(2-N)}\frac{\mathrm{d}p}{\mathrm{d}x}(h^4 + f(h)), \tag{30}$$

where

$$f(h) = \frac{4Nh}{m}\Big(\frac{(h/m)\mathrm{I}_1(mh) - (h^2/2)\mathrm{I}_0(mh)}{\mathrm{I}_1(mh)}\Big) + 2(2-N)h^3k_n. \tag{31}$$

From Eq. (30), the pressure gradient can be obtained as

$$\frac{\mathrm{d}p}{\mathrm{d}x} = -\frac{4(2-N)}{1-N}\Big(\frac{q+h^2}{h^4+f(h)}\Big). \tag{32}$$

Integrating Eq. (32) over one wavelength, we get

$$\Delta p = p_1 - p_0 = -\frac{4(2-N)}{1-N}(qL_1 + L_2), \tag{33}$$

where

$$L_1 = \int_0^1 \frac{\mathrm{d}x}{h^4+f(h)}, \quad L_2 = \int_0^1 \frac{h^2\mathrm{d}x}{h^4+f(h)}.$$

The non-dimensional time averaged flux ($\overline{Q}$) over one period in the fixed frame is given by

$$\overline{Q} = \frac{1}{T}\int_0^T (q+h^2)\mathrm{d}t \;=\; q + q_1, \tag{34}$$

where

$$q_1 = \int_0^1 h^2\mathrm{d}x.$$

From Eqs. (33) and (34), we get

$$\Delta p = -\frac{4(2-N)}{1-N}((\overline{Q}-q_1)L_1 + L_2) \tag{35}$$

or

$$\overline{Q} = q_1 - \frac{L_2}{L_1} - \frac{1-N}{4(2-N)}\frac{\Delta p}{L_1}. \tag{36}$$

The nonzero dimensionless shear stresses for the micro-polar fluid are given by

$$\tau_{zr} = \frac{\partial u}{\partial r} - \frac{N}{1-N}\omega, \tag{37}$$

$$\tau_{rz} = \frac{1}{1-N}\frac{\partial u}{\partial r} + \frac{N}{1-N}\omega. \tag{38}$$

The dimensionless friction force ($F$) on the inner wall of the tube by using Eq. (37) over one wavelength is obtained as

$$\begin{aligned} F \;&= -2\int_0^1 h(x)(\tau_{zr})_{r=h}\mathrm{d}x \\ &= -2\int_0^1 h(x)\Big(\frac{\partial u}{\partial r}\Big)_{r=h}\mathrm{d}x. \end{aligned} \tag{39}$$

Substituting the value of $u$ from Eq. (26) in Eq. (39) and using Eqs. (32) and (36), we get

$$\begin{aligned} F &= -(1-N)\int_0^1 h^2 \frac{\mathrm{d}p}{\mathrm{d}x}\mathrm{d}x \\ &= 4(2-N)\Big(L_3 - \frac{L_2^2}{L_1}\Big) - (1-N)\Delta p \frac{L_2}{L_1}, \end{aligned} \tag{40}$$

where

$$L_3 = \int_0^1 \frac{h^4}{h^4 + f(h)}\mathrm{d}x.$$

The mechanical efficiency is defined as the ratio between the average rate per wavelength, at which work is done by the moving fluid against a pressure head, and the average, at which the walls do work on the fluid (see Shapiro et al.[30]). The mechanical efficiency derived for micro-polar fluids is

$$E = \frac{\overline{Q}\Delta p}{2\pi\phi\big(-\int_0^1 \frac{\mathrm{d}p}{\mathrm{d}x}\sin(2\pi x)\mathrm{d}x - \frac{\phi}{4}\Delta p + \frac{\phi}{4}\int_0^1 \frac{\mathrm{d}p}{\mathrm{d}x}\cos(4\pi x)\mathrm{d}x\big)}. \tag{41}$$

## 3 Numerical results and discussion

Numerical results are obtained and presented in this section for studying the effects of the coupling number ($N$), the micro-polar parameter ($m$), and the slip parameter ($k_n$) on the pumping characteristic, the friction force at the wall of the tube, the velocity profile, the mechanical efficiency, and the trapping phenomenon. The case when the pressure rise is zero ($\Delta p = 0$) is called free pumping. In this case, the value of the averaged flux ($\overline{Q}$) is called the free pumping flux rate (or the maximum averaged flux rate), which is denoted by $\overline{Q}_0$. The maximum pressure difference, against which peristalsis can work, is denoted by $p_0$, which is the value of $\Delta p$ corresponding to $\overline{Q} = 0$. The cases when $0 < \Delta p \leqslant p_0$, $\Delta p < 0$, and $\Delta p = 0$ correspond to pumping, co-pumping, and free pumping, respectively. The regions for pumping, free pumping, and co-pumping are denoted as the pumping region, the free pumping region, and the co-pumping region, respectively.

The effects of $N$, $m$, and $k_n$ on the pressure with the averaged flux rate are shown in Figs. 1–3. From these figures, it is noted that the pumping region ($0 < \Delta p \leqslant p_0$) increases with the increase in the coupling number ($N$), while decreases with the increase in the magnitude of the micro-polar parameter ($m$) and the slip parameter ($k_n$). The effect of $k_n$ on the pressure is observed to be opposite to that of the effect of $N$ in qualitative sense. Moreover, the pumping

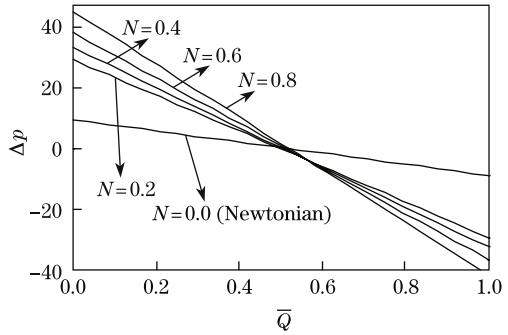


**Fig. 1** Pressure rise versus averaged flux rate for $\phi = 0.4$, $m = 2$, and $k_n = 0.00$

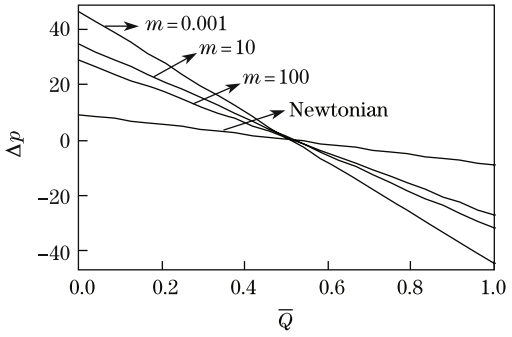


**Fig. 2** Pressure rise versus averaged flux rate for $\phi = 0.4$, $N = 0.8$, and $k_n = 0.00$

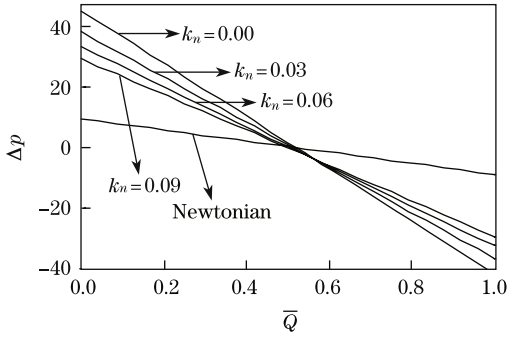


**Fig. 3** Pressure rise versus averaged flux rate for $\phi = 0.4$, $N = 0.8$, and $m = 2$

region of $0 < \Delta p \leqslant p_0$ is greater for micro-polar fluids in comparison with that for Newtonian fluids. Figure 1 also shows that the pressure increases in the region of $\overline{Q} \leqslant 0.48$ whereas reduces in the region of $\overline{Q} > 0.48$ with the increase in the magnitude of $N$. Figure 2 also shows that the pressure reduces in the region of $\overline{Q} \leqslant 0.48$ and increases in the region of $\overline{Q} > 0.48$ with the increase in the magnitude of $m$.

Tables 1–3 present the variation of the free pumping flux rate ($\overline{Q}_0$) with $N$, $m$, and $k_n$. It is found that $\overline{Q}_0$ increases with the increase in $N$ and decreases with the increase in $k_n$ (see Tables 1 and 3). Table 2 reveals that $\overline{Q}_0$ initially increases with the increase in $m$ up to a certain stage, and after then it decreases. The results obtained in this study, respectively, reduce to the results of Srinivasacharya et al.[3] when $k_n = 0.00$ and the results of Shapiro et al.[30] when $N = 0.0$ and $k_n = 0.00$.

**Table 1** Free pumping flux rate $\overline{Q}_0$ in free pumping region for different $N$ with $\phi = 0.4$, $m = 2$, and $k_n = 0.00$

| | $N$ | | | |
|---|---|---|---|---|
| | 0.0 | 0.4 | 0.6 | 0.8 |
| $\overline{Q}_0$ | 0.510 968 | 0.514 003 | 0.516 031 | 0.518 570 |

**Table 2** Free pumping flux rate $\overline{Q}_0$ in free pumping region for different $m$ with $\phi = 0.4$, $N = 0.4$, and $k_n = 0.00$

| | $m$ | | | |
|---|---|---|---|---|
| | 0.001 | 1 | 10 | 100 |
| $\overline{Q}_0$ | 0.510 968 | 0.512 014 | 0.515 575 | 0.511 606 |

**Table 3** Free pumping flux rate $\overline{Q}_0$ in free pumping region for different $k_n$ with $\phi = 0.4$, $m = 2$, and $N = 0.4$

| | $k_n$ | | | |
|---|---|---|---|---|
| | 0.00 | 0.03 | 0.06 | 0.09 |
| $\overline{Q}_0$ | 0.514 003 | 0.505 206 | 0.498 080 | 0.492 175 |

Figures 4–6 depict the effects of $N$, $m$, and $k_n$ on the friction force ($F$) with the averaged flux rate ($\overline{Q}$). From these figures, it is observed that there exists a critical value of $\overline{Q}$, below which $F$ resists the flow and above which $F$ assists the flow. This critical value of $\overline{Q}$ decreases with the increases in $N$ and $k_n$, and increases with the increase in $m$ (see Tables 4–6). Below

this critical value of $\overline{Q}$, the friction force $F$ increases when the magnitudes of $N$, $m$, and $k_n$ increase, while above this critical value of $\overline{Q}$, the friction force $F$ decreases when the magnitudes of $N$, $m$, and $k_n$ increase.

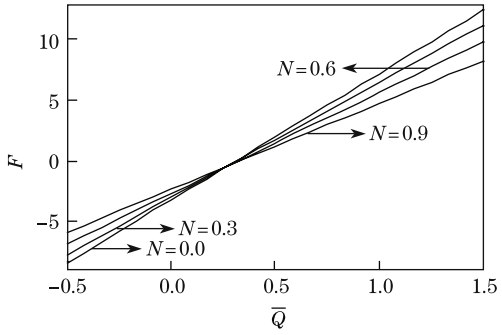


**Fig. 4** Friction force at wall versus averaged flux rate for $\phi = 0.4$, $m = 10$, and $k_n = 0.00$

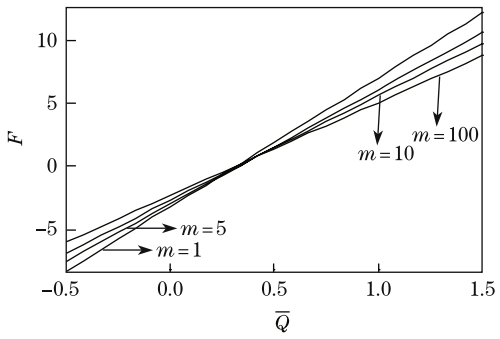


**Fig. 5** Friction force at wall versus averaged flux rate for $\phi = 0.4$, $N = 0.6$, and $k_n = 0.00$

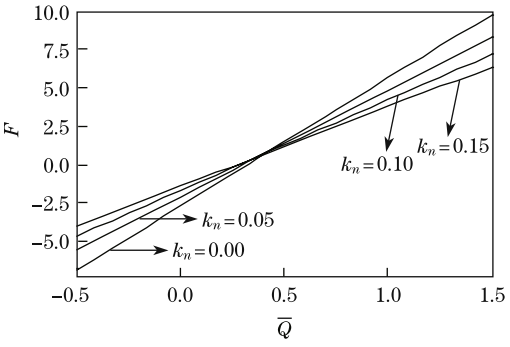


**Fig. 6** Friction force at wall versus averaged flux rate for $\phi = 0.4$, $N = 0.6$, and $m = 10$

**Table 4** Critical values of $\overline{Q}$ for different $N$ with $\phi = 0.4$, $m = 2$, and $k_n = 0.00$

| | $N$ | | | |
|---|---|---|---|---|
| | 0.0 | 0.4 | 0.6 | 0.8 |
| $\overline{Q}$ | 0.156 960 | 0.148 538 | 0.145 845 | 0.144 668 |

**Table 5** Critical values of $\overline{Q}$ for different $m$ with $\phi = 0.4$, $N = 0.4$, and $k_n = 0.00$

| | $m$ | | | |
|---|---|---|---|---|
| | 0.001 | 2 | 10 | 100 |
| $\overline{Q}$ | 0.140 145 | 0.148 538 | 0.159 460 | 0.157 375 |

**Table 6** Critical values of $\overline{Q}$ for different $k_n$ with $\phi = 0.4$, $m = 2$, and $N = 0.4$

| | $k_n$ | | | |
|---|---|---|---|---|
| | 0.00 | 0.03 | 0.06 | 0.09 |
| $\overline{Q}$ | 0.148 538 | 0.140 866 | 0.138 299 | 0.139 529 |

The influences of the pertinent parameters $N$, $m$, and $k_n$ on the velocity profile (curves between the radial displacement $r$ and the axial velocity $u$) are shown in Figs. 7–9. The relation between them is found to be non-linear, and the maximum velocity is achieved at zero radial displacement and vice-versa. The revelation is that the axial velocity diminishes with the increase in the magnitude of the coupling number and the slip parameter whereas increases with the increase in the magnitude of the micro-polar parameter. This indicates that the region of the velocity profile reduces with the increase in the magnitudes of $N$ and $k_n$ whereas enhances with the increase in the magnitude of $m$.

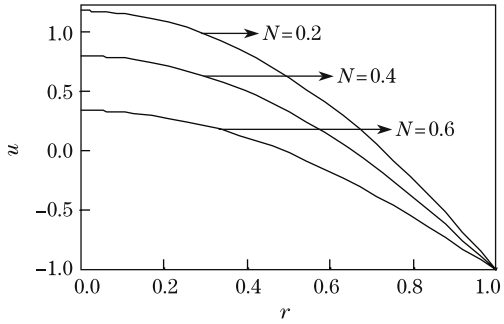


**Fig. 7** Axial velocity versus radial distance for $\phi = 0.4$, $k_n = 0.00$, $m = 10$, $x = 0.5$, and $\mathrm{d}p/\mathrm{d}x = -10$

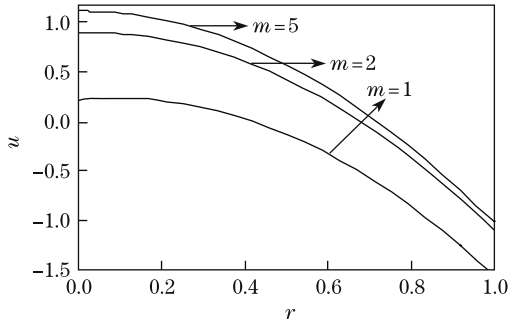


**Fig. 8** Axial velocity versus radial distance for $\phi = 0.4$, $k_n = 0.00$, $N = 0.2$, $x = 0.5$, and $\mathrm{d}p/\mathrm{d}x = -10$

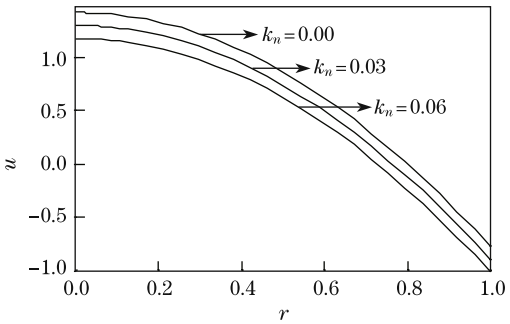


**Fig. 9** Axial velocity versus radial distance for $\phi = 0.4$, $N = 0.2$, $m = 10$, $x = 0.5$, and $\mathrm{d}p/\mathrm{d}x = -10$

The curves between the mechanical efficiency $E$ and the ratio of the averaged flux rate and the maximum averaged flux rate $\overline{Q}/\overline{Q}_0$ are plotted in Fig. 10 to show the effects of the parameters $N$, $m$, and $k_n$. It is observed that $E$ first increases, attains a maximum value, and then decreases to zero. It is also found that the mechanical efficiency increases with the increase in the magnitude of the coupling number, while decreases with the increases in the micro-polar parameter and the slip parameter.

Trapping is an inherent phenomenon of peristaltic motion, in which an internally circulating bolus of fluids is formed by closed streamlines. This trapped bolus is pushed ahead along with the peristaltic wave. The effects of the coupling number $N$, the micro-polar parameter $m$, and the slip parameter $k_n$ can be seen through Figs. 11–13. It is observed regarding the effects of $N$ and $m$ that the trapped bolus increases in the size as $N$ and $m$ increase, while the size of the trapped bolus reduces as $k_n$ increases.

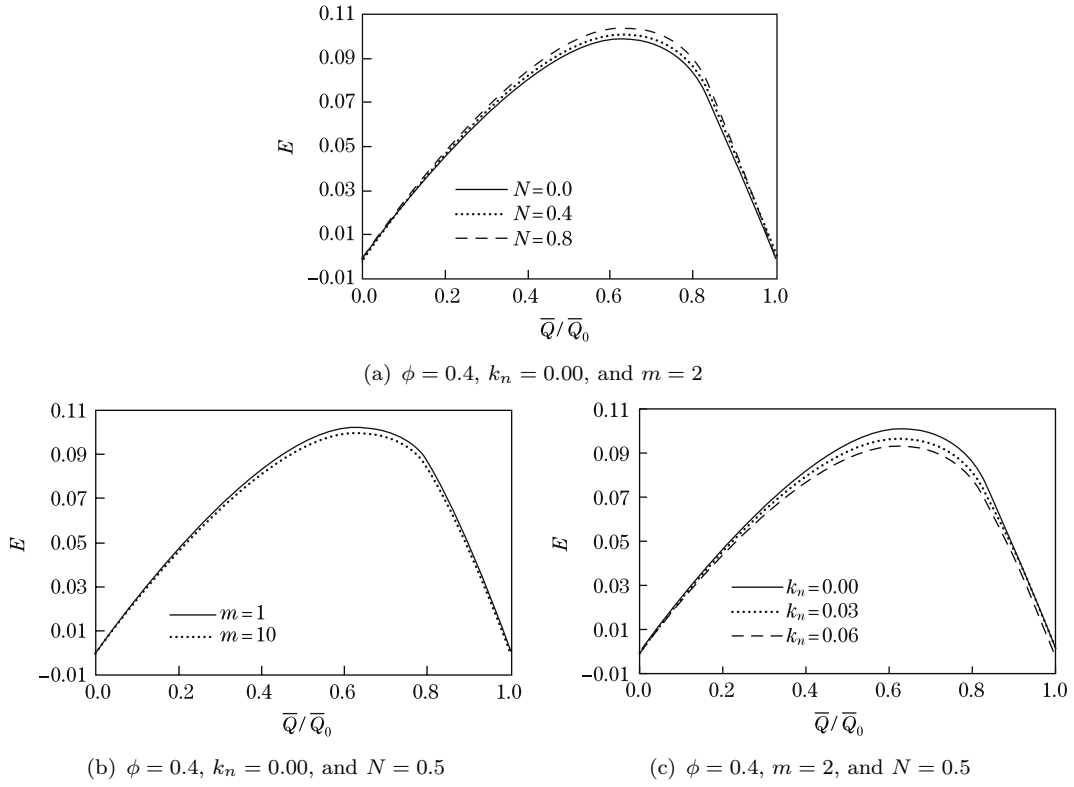


(a) $\phi = 0.4$, $k_n = 0.00$, and $m = 2$

(b) $\phi = 0.4$, $k_n = 0.00$, and $N = 0.5$

(c) $\phi = 0.4$, $m = 2$, and $N = 0.5$

**Fig. 10** Mechanical efficiency versus ratio of averaged flux rate and maximum averaged flux rate with different papameters

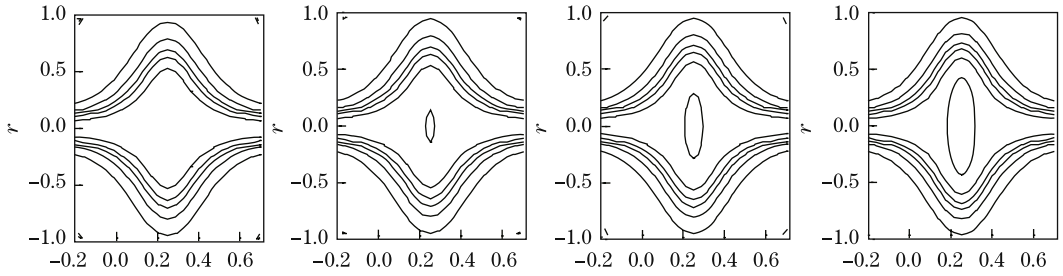


(a) $N$=0.0 (b) $N$=0.1 (c) $N$=0.4 (d) $N$=0.8

**Fig. 11** Streamlines for $m = 2$, $\phi = 0.4$, $k_n = 0.00$, and $\overline{Q} = 0.1$

## 4 Conclusions

The effects of the coupling number ($N$), the micro-polar parameter ($m$), and the slip parameter ($k_n$) on the pumping region, the friction force at the wall, the velocity profile, the mechanical efficiency, and the trapping phenomenon are discussed numerically in detail. The main findings of the present study are as follows:

(i) The peristaltic pumping region narrows down by increasing the micro-polar parameter ($m$) and the slip parameter ($k_n$), while widens by increasing the coupling number ($N$).

(ii) The critical value of $\overline{Q}$, below which $F$ resists the flow and above which $F$ assists the

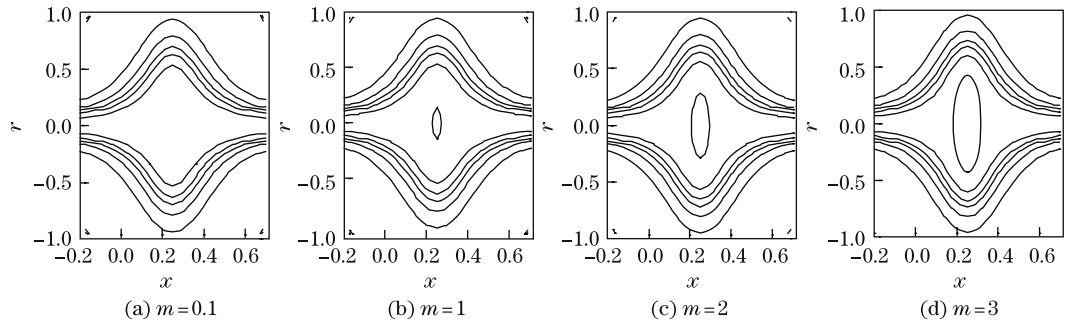


(a) $m=0.1$ (b) $m=1$ (c) $m=2$ (d) $m=3$

**Fig. 12** Streamlines for $N = 0.8$, $\phi = 0.4$, $k_n = 0.00$, and $\overline{Q} = 0.1$

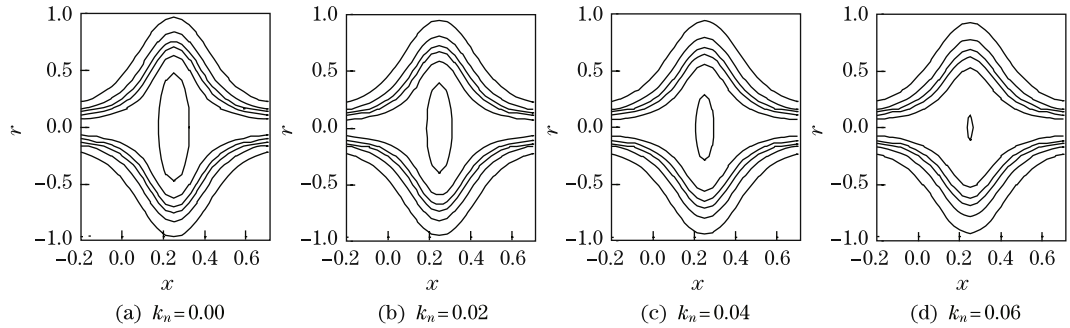


(a) $k_n=0.00$ (b) $k_n=0.02$ (c) $k_n=0.04$ (d) $k_n=0.06$

**Fig. 13** Streamlines for $N = 0.8$, $\phi = 0.4$, $m = 3.0$, and $\overline{Q} = 0.1$

flow, decreases with the increases in $N$ and $k_n$, and increases with the increase in $m$.

(iii) The magnitude of the axial velocity reduces with the increases in $N$ and $k_n$ whereas increases with the increase in $m$.

(iv) The mechanical efficiency enhances with increasing $N$ while diminishes with increasing $m$ and $k_n$.

(v) The size of the trapped bolus increases by increasing $N$ and $m$ while decreases by increasing $k_n$.

(vi) The results for micropolar fluids (Srinivasacharya et al.[3]) and Newtonian fluids (Shapiro et al.[30]) without the slip boundary condition (i.e., no slip condition) can be obtained as the special cases of the present analysis by taking $k_n = 0.00$ and $N = 0.0$, $k_n = 0.00$, respectively.

## References

[1] Eringen, C. Theory of micropolar fluids. *Journal of Mathematics and Mechanics*, **16**, 1–16 (1966)

[2] Devi, R. G. and Devanathan, R. Peristaltic motion of a micropolar fluid. *Proceedings of the Indian Academy of Sciences*, **81**, 149–163 (1975)

[3] Srinivasacharya, D., Mishra, M., and Rao, A. R. Peristaltic pumping of a micropolar fluid in a tube. *Acta Mechanica*, **161**, 165–178 (2003)

[4] Muthu, P., Kumar, B. V. R., and Chandra, P. Peristaltic motion of micropolar fluid in circular cylindrical tubes: effect of wall properties. *Applied Mathematical Modeling*, **32**, 2019–2033 (2008)

[5] Hayat, T. and Ali, N. Effects of an endoscope on peristaltic flow of a micropolar fluid. *Mathematical and Computer Modelling*, **48**, 721–733 (2008)

[6] Hayat, T., Ali, N., and Abbas, Z. Peristaltic flow of micropolar fluid in a channel with different wave forms. *Physics Letters A*, **370**, 331–344 (2007)

[7] Muthu, P., Kumar, B. V. R., and Chandra, P. On the influence of wall properties in the peristaltic motion of micropolar fluid. *ANZIAM Journal*, **45**, 245–260 (2003)

[8] Ali, N. and Hayat, T. Peristaltic flow of a micropolar fluid in an asymmetric channel. *Computers and Mathematics with Applications*, **55**, 589–608 (2008)

[9] Mekheimer, K. S. and Elmaboud, Y. A. The influence of a micropolar fluid on peristaltic transport in an annulus: application of the clot mode. *Applied Bionics and Biomechanics*, **5**, 13–23 (2008)

[10] Pandey, S. K. and Tripathi, D. A mathematical model for peristaltic transport of micro-polar fluids. *Applied Bionics and Biomechanics*, **8**, 279–293 (2011)

[11] Pandey, S. K. and Chaube, M. K. Peristaltic flow of a micropolar fluid through a porous medium in the presence of an external magnetic field. *Communications in Nonlinear Science and Numerical Simulations*, **16**, 3591–3601 (2011)

[12] Kwang, W., Chu, H., and Fang, J. Peristaltic transport in a slip flow. *European Physical Journal B*, **16**, 543–547 (2000)

[13] Hakeem, A. E., Naby, A. E., and Shamy, I. I. E. Slip effects on peristaltic transport of power-law fluid through an inclined tube. *Applied Mathematical Sciences*, **60**, 2967–2980 (2007)

[14] Ali, N., Hussain, Q., Hayat, T., and Asghar, S. Slip effects on the peristaltic transport of MHD fluid with variable viscosity. *Physics Letters A*, **372**, 1477–1489 (2008)

[15] Hayat, T., Qureshi, M. U., and Ali, N. The influence of slip on the peristaltic motion of a third order fluid in an asymmetric channel. *Physics Letters A*, **372**, 2653–2664 (2008)

[16] Tripathi, D., Gupta, P. K., and Das, S. Influence of slip condition on peristaltic transport of a viscoelastic fluid with fractional Burgers' model. *Thermal Science*, **15**(2), 501–515 (2011)

[17] Pandey, S. K. and Tripathi, D. Influence of magnetic field on the peristaltic flow of a viscous fluid through a finite-length cylindrical tube. *Applied Bionics and Biomechanics*, **7**, 169–176 (2010)

[18] Pandey, S. K. and Tripathi, D. Peristaltic flow characteristics of Maxwell and magneto-hydrodynamic fluids in finite channels. *Journal of Biological Systems*, **18**, 621–647 (2010)

[19] Pandey, S. K. and Tripathi, D. Unsteady model of transportation of Jeffrey fluid by peristalsis. *International Journal of Biomathematics*, **3**, 453–472 (2010)

[20] Pandey, S. K. and Tripathi, D. Peristaltic transport of a casson fluid in a finite channel: application to flows of concentrated fluids in oesophagus. *International Journal of Biomathematics*, **3**, 473–491 (2010)

[21] Tripathi, D., Pandey, S. K., and Das, S. Peristaltic transport of a generalized Burgers' fluid: application to movement of chyme in small intestine. *Acta Astronautica*, **69**, 30–38 (2011)

[22] Tripathi, D. Numerical and analytical simulation of peristaltic flows of generalized Oldroyd-B fluids. *International Journal for Numerical Methods in Fluids*, DOI 10.1002/fld.2466

[23] Tripathi, D. Peristaltic transport of a viscoelastic fluid in a channel. *Acta Astronautica*, **68**, 1379–1385 (2011)

[24] Tripathi, D. Numerical study on peristaltic flow of generalized Burgers' fluids in uniform tubes in presence of an endoscope. *International Journal for Numerical Methods in Biomedical Engineering*, **27**(11), 1812–1828 (2011)

[25] Tripathi, D. Peristaltic transport of fractional Maxwell fluids in uniform tubes: application of an endoscope. *Computers and Mathematics with Applications*, **62**(3), 1116–1126 (2011)

[26] Tripathi, D. Numerical study on peristaltic transport of fractional bio-fluids. *Journal of Mechanics in Medicine and Biology*, DOI 10.1142/S0219519411004290

[27] Tripathi, D., Pandey, S. K., and Das, S. Peristaltic flow of viscoelastic fluid with fractional Maxwell model through a channel. *Applied Mathematics and Computation*, **215**, 3645–3654 (2010)

[28] Pandey, S. K. and Chaube, M. K. Peristaltic transport of a visco-elastic fluid in a tube of non-uniform cross section. *Mathematical and Computer Modelling*, **52**, 501–514 (2010)

[29] Pandey, S. K. and Chaube, M. K. Study of wall properties on peristaltic transport of a couple stress fluid. *Meccanica*, DOI 10.1007/s11012-010-9387-8

[30] Shapiro, A. H., Jafferin, M. Y., and Weinberg, S. L. Peristaltic pumping with long wavelengths at low Reynolds number. *Journal of Fluid Mechanics*, **37**, 799–825 (1969)